Journal of Molecular Structure: THEOCHEM xxx (2009) xxx–xxx

Contents lists available at ScienceDirect

Journal of Molecular Structure: THEOCHEM

journal homepage: www.elsevier.com/locate/theochem

DFT RX3LYP and RPBEPBE studies on the structural, electronic, and vibrational properties of some amino-alcohol ligands

Pradeep R. Varadwaj [a,1], Ignacy Cukrowski [a,*], Helder M. Marques [b,*]

[a] Department of Chemistry, Natural & Agricultural Sciences 1, University of Pretoria, Lynnwood Road, Pretoria 0002, South Africa
[b] Molecular Sciences Institute, School of Chemistry, University of the Witwatersrand, Johannesburg 2050, South Africa

ARTICLE INFO

Article history:
Received 29 April 2009
Accepted 10 August 2009
Available online xxxx

Keywords:
Amino-alcohol ligands
DFT calculation
QTAIM critical point analysis
NBO
Hydrogen bonding
IR and Raman spectra

ABSTRACT

To rationalize the influence of molecular architecture on metal ion selectivity and affinity, a DFT study of three amino-alcohol ligands, bis(2-hydroxyethyl)-ethane-1,2-diamine (BHEEN), and two ligands where the backbone is reinforced with cycloalkyl moieties, *N,N′*-bis(2-hydroxycyclopentyl)-ethane-1,2-diamine (Cyp_2-EN), and *N,N′*-bis(2-hydroxycyclohexyl)-ethane-1,2-diamine (Cy_2-EN), using the X3LYP and PBEPBE functionals with 6-31G(d,p), 6-31+G(d,p) and 6-311++G(d,p) basis sets has been conducted in combination with Quantum Theory of Atoms in Molecules (QTAIM) and Natural Bond Orbital (NBO) analyses. QTAIM analysis predicted the formation of intra-molecular N–H···O–H and –H···H– interactions only in Cy_2-EN. The latter interaction in metal complexes is often interpreted as a destabilizing steric repulsion. These analyses also predicted the electron density at the ring critical point, and its Laplacian, of the cyclopentyl moiety in Cyp_2-EN to be twice as large as those of the cyclohexyl moiety in Cy_2-EN. It is suggested that the increased electron density within the 5-member reinforcement rings is responsible for the absence of the intramolecular interactions observed in Cy_2EN and also contributes to its lower affinity for metal ions. The formation of the intramolecular N–H···O–H bond was observed in the NBO analysis for all three ligands since values of the second-order stabilization energy $E^{(2)}$ caused by the charge transfer between the O lone-pair and the N–H bond was non-zero. The strength of the H-bond increased in the order Cy_2-EN > BHEEN > Cyp_2-EN that is consonant with a decrease in the N–H···O–H distance. Because a similar trend, *viz.*, log K_{ML}(Cy_2-EN) > log K_{ML}(BHEEN) > log K_{ML}(Cyp_2-EN) is observed for the stability constants with all metal ions, we tentatively conclude that the ability of the ligand to transfer charge between orbitals, as described by $E^{(2)}$, is a factor that influences the ligand's ability to form complexes. A comparison between the calculated results (structure, vibrational spectra) and experimental results are used to validate the conclusions.

1. Introduction

Interest in the chemistry of amino-alcohols stems, *inter alia*, from their importance in the pharmaceutical industry [1–3], their use as chiral reagents in organic synthesis [4–6], especially as a Zn(II) complex [7,8], and as cross-linking reagents in the synthesis of precursor systems for superconductors [9,10]. Amino-alcohols could play an important role in medicinal chemistry as ligands for metals in complexes that are alternatives to presently administered agents in diagnostic and curative protocols. Towards this end, an understanding of their coordination behavior is important.

We are interested in amino-alcohols which contain at least two N- and two O-donor atoms, as ligands for a variety of transition and inner transition metal ions. A simple example of such a ligand is the commercially available potentially tetradentate ligand *N,N′*-bis(2-hydroxyethyl)-ethane-1,2-diamine (BHEEN) (Scheme 1A). De Sousa and Hancock [11,12] have shown that, by the appropriate manipulation of reaction conditions, the reaction of 1*R*,2*S*-cyclohexene oxide with a diamine or a triamine produces predominantly the *meso* form (1*R*,2*R*,1′*S*,2′*S*) of a product with two pendent cyclohexanol groups typically in 70–80% yield. This was found in the case of the ligands *N,N′*-bis(2-hydroxycyclohexyl)-trans-cyclohexane-1,2-diamine (TCA), *N,N′*-bis(2-hydroxycyclohexyl)-propane-1,3-diamine (Cy_2-tn) and *N′,N″*-bis(2-hydroxycyclohexyl)-1,4,7-triazaheptane (Cy_2-dien) (Scheme 1B). Recently the *meso* form of the related ligands *N,N′*-bis(2-hydroxycyclohexyl)-ethane-1,2-diamine (Cy_2-EN), *N,N′*-bis(2-hydroxycyclopentyl)-ethane-1,2-diamine (Cyp_2-EN) and *N,N′*-bis(2-hydroxycyclohexyl)-propan-2-ol-1,3-diamine (Cy_2-otn) (Scheme 1B and C) has been prepared [13].

* Corresponding authors.
E-mail addresses: Ignacy.Cukrowski@up.ac.za (I. Cukrowski), Helder.Marques@wits.ac.za (H.M. Marques).
[1] Present address: Department of Chemistry, Faculty of Sciences, Okayama University, Tusima-naka 3-1-1, Okayama-Shi, Okayama-ken 700-8530, Japan.

0166-1280/$ - see front matter © 2009 Elsevier B.V. All rights reserved.
doi:10.1016/j.theochem.2009.08.009

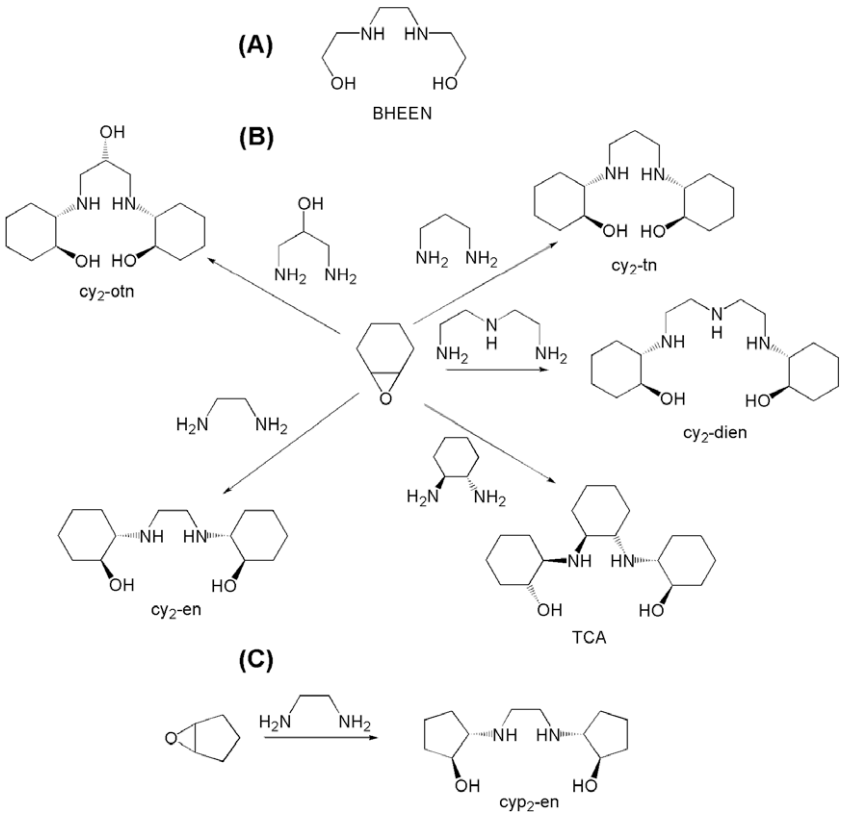

Scheme 1.

The properties of ligands, and in particular their preferred coordination behavior, often can be modified and fine tuned by simple structural modifications [14]; for instance, N-donor ligands that have also neutral oxygen donors incorporated show an increased selectivity for larger metal ions relative to smaller metal ions [15]; however, this fundamental concept in ligand design can be modified. For example, if an ethyl bridge between the N- and O-donors is replaced by a cyclohexyl bridge, the ligand becomes selective towards smaller metal ions [12,16–18]. Based largely on a molecular mechanics analysis, this has been attributed [19] to short repulsive contacts between H-atoms on the cyclohexyl bridges and H-atoms on the backbone of the ligand; these repulsive contacts become shorter with increasing metal-ion size and hence increased selectivity for smaller metal ions is observed.

The focus in this work is on BHEEN (it contains a simple ethyl bridge between the N- and O-donor atoms and therefore it has no "structural reinforcement") and on the structurally reinforced analogues Cyp_2-EN and Cy_2-EN with cyclopentyl and cyclohexyl bridges, respectively, between the N- and O-donor atoms. We refer to these ligands as containing "5-membered reinforcement rings" (5m-RR) and "6-membered reinforcement rings" (6m-RR). The stability constants, as log K_{ML} values, for the formation of a 1:1 complex between the metal and the ligand have been reported to be 3.79 and 7.75 for Ni(II) with Cyp_2-EN and Cy_2-EN, respectively [20], or $\Delta\log K_{ML} = 3.96$, which is over 100% increase in log K value due to the change from 5m-RR to 6m-RR added to the ligand BHEEN (Table 1). Ni(II) (ionic radius $r = 0.69$ Å) is a medium-size ion. With Cu(II), which is a smaller metal ion ($r = 0.57$ Å) the analogous increase in log K is only 67% (6.75 and 11.29, respectively). The addition to BHEEN of (i) a 5m-RR to form Cyp_2-EN results in the decrease in stability constants of ML by about 30 and 43% for Cu(II) and Ni(II), respectively, and (ii) a 6m-RR to form Cy_2-EN increases the stability constants for Cu(II) and Cd(II) (ionic radius $r = 0.95$ Å) by about 17 and 21%, respectively. Hence the rule of preferred selectivity towards small metal ions [12,16–18] seems to have been violated. It would appear that rationalizations based on steric interactions between backbone H-atoms, a "steric repulsion" argument founded on a classical mechanics model, may not be adequate to explain such experimental observations. We therefore have decided to focus on DFT modeling of these ligands and their complexes.

Table 1
Stability constants (as log K_{ML}) for the formation of 1:1 complexes between several amino-acid ligands and selected metal ions in aqueous solution, $\mu = 0.1$ M $(H^+,Na^+)NO_3^-$, 25 °C. Data from [20].

M	r (Å)	log K_{ML}		
		Cyp_2-EN	BHEEN	Cy_2-EN
Cu(II)	0.57	6.75	9.68	11.29
Ni(II)	0.69	3.70	6.67	7.75
Cd(II)	0.95	3.98	5.07	6.15

Our ultimate aim is to model metal ion complexes with amino-alcohol ligands to rationalize the influence of the ligand architecture on metal ion selectivity and affinity as well as to theoretically predict experimentally-determined stability constants. Towards this end, it is important to understand the structural, electronic, and vibrational properties of ligands and to identify the presence of weak intramolecular interactions if any. Our attention in particular was focused on (i) the formation of bond paths in which the donor atoms might be involved as this would be expected to control and modify their coordination properties, (ii) the influence of a small structural change from 5m-RR to 6m-RR on the electronic properties and hence the formation of preferential bond paths in these ligands, and (iii) whether there is a correlation between the structural and physical properties (as in (i) and (ii) above) and

the ligands' ability to form complexes as measured by the experimental complex formation constants. In this work, we have therefore undertaken DFT studies of the three representative ligands, BHEEN, Cyp_2-EN, and Cy_2-EN using X3LYP and PBEPBE functionals in conjunction with three basis sets, 6-31G(d,p), 6-31+G(d,p) and 6-311++G(d,p) in the gas phase and in simulated solvent (as water) in anticipation that this may provide better insight into factors that control complex stability and ligand selectivity. The physical parameters resulting from this calculation were analyzed and compared. We were interested in whether the choice of functional and basis set had an influence on identifying properties of these ligands, which might explain their differential ability to complex metal ions. Since QTAIM provides a great deal of information about the nature of the bonding environment, we have explored the topological properties of the electron charge density and the Laplacian of the charge density at various bond critical points using the Quantum Theory of Atoms in Molecules (QTAIM) of Bader [21] to characterize the presence of possible open shell and close shell interactions. Furthermore, the natural population bond orbital technique has been applied to these systems for calculating the second-order stabilization energy $E^{(2)}$ of weak interactions caused by a charge transfer mechanism to estimate their strengths. A comparison between the calculated results (structure, vibrational spectra) and experimental results are used to validate the conclusions.

2. Experimental

2.1. Computational details

Unless otherwise indicated, all calculations were performed using Gaussian 03 [22] on a Linux workstation in parallel environment; visualization and assignments of the normal vibrational modes were performed with the help of the GaussView 03 suite of programs [23].

Two correlated DFT functionals, X3LYP (a hybrid GGA type that is an admixture of the Becke extended three-parameter (X3) exchange functional [24–26] coupled with the Lee–Yang–Parr electron-correlation functional [27]) and PBEPBE (an admixture of a GGA-type exchange and correlations of Perdew, Burke and Ernzerhof [28,29]) were used. These two functionals were employed in conjunction with three basis sets, 6-31G(d,p), 6-31+G(d,p) and 6-311++G(d,p), to investigate the equilibrium bond lengths and valence bond angles, the topology of the electron density and the vibrational properties of the three amino-alcohol ligands, BHEEN, Cyp_2-EN, and Cy_2-EN (Scheme 1). It is known that both standard and hybrid exchange-correlation functionals can be used for modeling the structures and properties of chemical systems with acceptable accuracy [30–34] and the B3LYP hybrid functional is one of the many such functionals which has been extensively applied. It has been suggested, however, that the B3LYP functional is inadequate for the description of weak interactions in chemical systems (and this is what we expected to be present in our ligands) because of the lack of electron–electron correlation [35–37]. The inclusion of electron correlation, as well as the use of flexible and extended basis sets augmented with diffuse functions, is important for accurately describing H-bonding and van der Waals interactions [38–41] since the choice of basis set influences not only the relative energetic stability of conformers, but also the number of local minima, and that is important in correctly analyzing the low energy barriers to internal rotation [42,43]. An extension to B3LYP, called X3LYP, addresses this issue to some extent. We have chosen this methodology because it is known to describe weak inter- and intra-molecular interactions [24,28,44,45] and the structure and electronic properties of molecular systems [24,45–47] in a well-defined manner. We used two different functionals to evaluate to what extent the computed thermochemical and electronic properties were dependent on the type of functional used.

Since one of the ultimate aims of our calculations is to rationalize and to predict stability constants of these three ligands with a variety of metal ions in aqueous solution, we therefore also investigated the effect of solvation on the structural, electronic and vibrational properties of each ligand. For this purpose we have used the self-consistent reaction field (SCRF) technique [48–51] in which the statistically averaged effect of the solvent is simulated by representing the medium with appropriate physical properties, such as the dielectric permittivity (ε) and the coefficient of thermal expansion. Dielectric continuum theories [52–55] are widely used to describe hydration because accurate results are produced at a relatively low computational cost; we have used the Conductor-like Polarizable Continuum Model (CPCM) [56–60] in conjunction with the united atom (UA) cavity-model in-tagged with Kohn–Sham (KS) radii (UAKS) [61,62]; the radii were optimized with PBEPBE/6-31G(d,p) with solvent as water ($\varepsilon = 78.39$) for this purpose. For the calculations involving the simulation of solvent we set TSARE = 0.3 and TSNUM = 100 in order to avoid the oscillatory behavior often encountered during optimization.

The crystal structures of the ligands were available to us and hence their conformation in the solid state is known, but it is reasonable to expect that they will adopt a range of conformations in solution or, germane to this study, in the gas phase. In an attempt to find the minimum energy gas phase conformation, the conformational space of the ligands was explored by performing molecular dynamics and simulated annealing (MD/SA) molecular mechanics (MM) calculations using the Generalized AMBER Force Field (GAFF) of Kollman et al. [63], parameters for which we have added to the HYPERCHEM suite of programs [64]. Partial charges on the atoms were determined from a semi-empirical single point calculation using the PM3 model [65] at the crystal structure geometry. In a typical MD/SA simulation, the molecule was heated from 0 to 800 K over 20 ps in steps of 0.5 fs, maintained at 800 K for a time (between 1 and 20 ps) and then annealed to 0 K over 20 ps, followed by full energy minimization (Polak–Ribiere algorithm with a convergence criterion of 0.005 kcal mol^{-1} $Å^{-1}$ in the gradient.) This was repeated 20 times. For each ligand a few simulations were run with longer simulation times (between 100 and 500 ps) but returned structures were very similar to those already discovered.

The lowest energy structures, as well as several others, obtained from the MD/SA calculations for all three ligands were optimized by DFT methods as described above. We found no consistency between the MD/SA minimum energy structures and those obtained by DFT calculations. We therefore used the conformation of each ligand found in the solid state (ligands are located at an inversion center, C_i symmetry) as the starting structure for our DFT calculations. The structure of the three ligands was energy-optimized at both levels of theory in their electronic ground states. The calculations of the normal mode frequencies were performed with the aid of analytical second derivatives of the X3LYP and PBEPBE potential energy surfaces to locate genuine stationary points. A tight convergence criterion (10^{-5} hartee $bohr^{-1}$) with ultrafine integration grid was used instead of the default settings. The resulting output from Gaussian 03 with IMAG = 0 ensures that the stationary points for all the structures belong to true minima.

We carried out a topological analysis of the electron charge density ($\rho(r)$) and the Laplacian of the charge density ($\nabla^2\rho(r)$) at all the bond critical points (BCPs) using both X3LYP and PBEPBE in conjunction with the three different basis sets on the optimized molecular geometry of the ligands using the quantum theory atoms in molecules (QTAIM) of Bader [21]. For reasons discussed below, we focused on the results obtained using a 6-31G(d,p) basis set for the ligands both in the gas phase and in solution. The resulting formatted check point and wavefunction files were

used as inputs both to AIMALL [66] and AIM2000 [67,68] suite of programs for the calculation and visualization of the topological properties of $\rho(r)$ and $\nabla^2\rho(r)$.

Natural Bond Orbital (NBO) analyses has been applied successfully to a number of intra-molecular H-bonded systems [69–71]. We assessed the transfer of electron density between the electron donor and the acceptor of an idealized Lewis structure into an empty non-Lewis orbital by computing the second-order stabilization energies $E^{(2)}$ (caused by charge transfer interactions between various donor-acceptor pairs of orbitals) by natural localized molecular orbitals (NLMO) analysis using the NBO 3.0 set of programs [72,73] available in GAUSSIAN 03.

The wavefunctions were analyzed with the help of NBOs using the SCF density. Eq. (1) gives the second-order perturbative estimates of the energies $E^{(2)}$ associated with the delocalization $i \rightarrow j$ where q_i is the donor orbital occupancy, $F(i,j)$ is the off diagonal NBO Fock matrix element, ε_i and ε_j are the diagonal elements representing the orbital energies, and i,j represents donor NBO(i) and acceptor NBO(j), respectively.

$$E^{(2)} = \Delta E_{ij} = q_i F(i,j)^2/(\epsilon_i - \epsilon_j) \quad (1)$$

2.2. Materials and methods

BHEEN (as the unprotonated ligand) was obtained from Sigma–Aldrich and used as received. As will be described elsewhere [13], diffraction-quality crystals were obtained of its nitrate salt; crystals of the free ligand were not suitable for diffraction studies. Cyp_2-EN and Cy_2-EN were prepared by the method of de Sousa and Hancock [11,12] and good quality crystals of the neutral ligand were obtained. Their Raman spectra were measured using a Bruker 100 IFS FT-Raman spectrometer with a liquid N_2-cooled Ge detector and Nd:YAG laser (1064 nm excitation line) in the region 100–3500 cm^{-1} with approximately 300 mW power at the sample. The spectral resolution was 4 cm^{-1}; 256 scans were averaged for each spectrum. A DIGILAB FT-IR FTS 7000 Series spectrometer with WinIR Pro Version 3.4.2.021 software, ceramic IR source, a diamond ATR, and DTGS detector was used to record the IR spectra (32 averaged sample and background scans) in the range from 500 to 4500 cm^{-1} with a resolution of 4 cm^{-1}.

3. Results and discussion

3.1. Comparison of selected structural metrics from DFT calculations and the solid state structures

Fig. 1 shows the energy-minimized structures (X3LYP/6-311++G(d,p)) obtained in this study. In Tables 2 and 3 we compare the differences between the average bond lengths and bond angles of the solid state structures and the computed structures where the latter have been obtained using two different functionals and three basis sets; also included in the tables are values obtained from the CPCM/UAKS technique to simulate the effect of aqueous solvent.

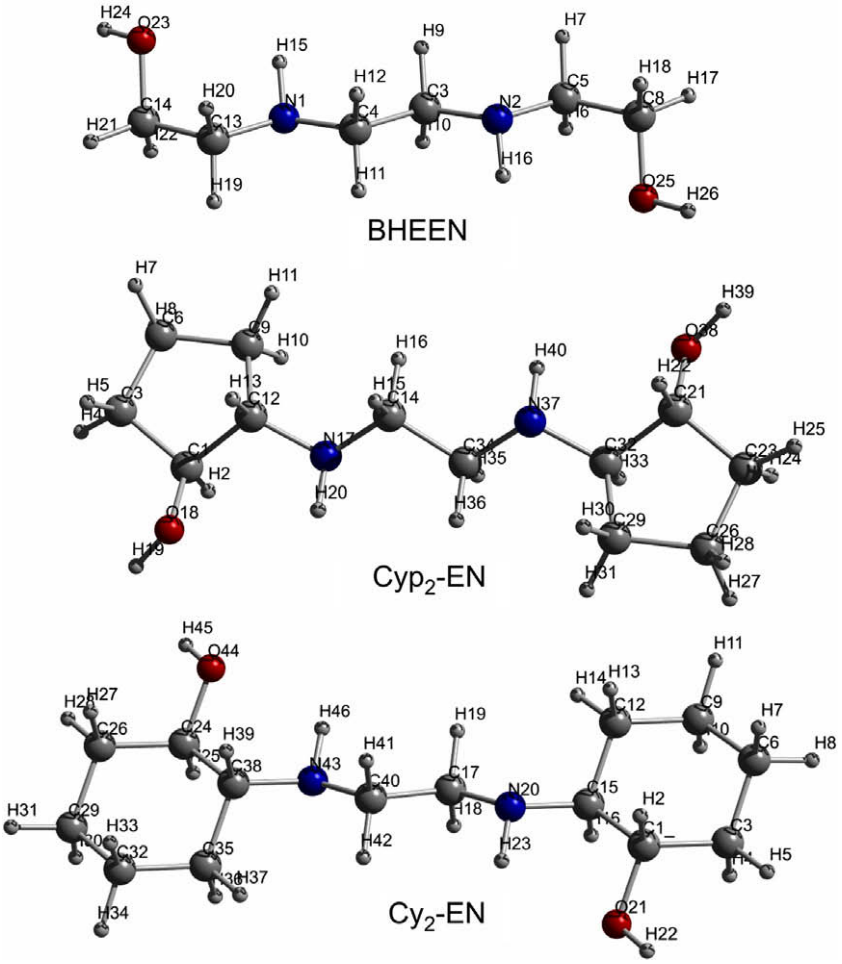

Fig. 1. Atomic numbering and energy-minimized structures obtained at the X3LYP/6-311++G(d,p) level of theory for the three amino-alcohol ligands studied in this work.

Table 2
Differences (calculated − observed) in the averages of selected bond lengths between the DFT-determined structures in gas phase (GP) and solvent (CPCM) of three amino-alcohols and the crystallographically determined structures.

Bond lengths (Å)	C–O		C–N		C–C	
	GP	CPCM	GP	CPCM	GP	CPCM
DHEEN[a]						
Experimental	1.415(2)		1.486(5)		1.513(6)	
X3LYP						
6-31G(d,p)	0.012		−0.029		0.010	
6-31+G(d,p)	0.018	0.022	−0.027	−0.020	0.010	0.010
6-311++G(d,p)	0.017	0.021	−0.028	−0.021	0.008	0.008
PBEPBE						
6-31G(d,p)	0.019		−0.025		0.014	
6-31+G(d,p)	0.026	0.028	−0.023	−0.016	0.014	0.013
6-311++G(d,p)	0.025	0.028	−0.025	−0.017	0.011	0.011
Cyp_2-EN						
Experimental	1.4167(11)		1.469(4)		1.529(10)	
X3LYP						
6-31G(d,p)	0.006		−0.011		0.011	
6-31+G(d,p)	0.012	0.015	−0.008	−0.002	0.013	0.011
6-311++G(d,p)	0.011	0.014	−0.009	−0.003	0.009	0.009
PBEPBE						
6-31G(d,p)	0.013		−0.006		0.014	
6-31+G(d,p)	0.020	0.022	−0.004	0.003	0.014	0.015
6-311++G(d,p)	0.019	0.022	−0.005	0.001	0.012	0.012
Cy_2-EN						
Experimental	1.418(2)		1.471(1)		1.521(3)	
X3LYP						
6-31G(d,p)	0.013		−0.008		0.012	
6-31+G(d,p)	0.019	0.020	−0.007	−0.001	0.013	0.012
6-311++G(d,p)	0.018	0.021	−0.008	−0.001	0.011	0.011
PBEPBE						
6-31G(d,p)	0.021		−0.004		0.015	
6-31+G(d,p)	0.027	0.029	−0.002	0.004	0.016	0.016
6-311++G(d,p)	0.027	0.029	−0.004	0.003	0.013	0.014

[a] The solid state structure is that of the nitrate salt; calculations were performed on the neutral molecule.

The actual values themselves, and not just the differences, are given in Table S1 of the Supplementary Information.

The DFT calculations and the crystal structure of BHEEN are not directly comparable because the structure of the unprotonated ligand is not available whilst, since we wished to compare the structures and intramolecular interactions of the three ligands in question, our calculations were confined to the unprotonated ligand. The results for both Cyp_2-EN and Cy_2-EN indicate that the DFT methods employed predicted bond lengths well. The analysis of data seen in Table 2 indicates that both functionals tend to slightly overestimate C–O and C–C bond lengths (typically by up to 0.02 Å), but the C–N bond lengths are reproduced to better than 0.01 Å. Interestingly, the smallest basis set used (6-31G(d,p)) predicted the C–O bond lengths most accurately for optimizations conducted in the gas phase for both functionals; the calculated C–C and C–N bond lengths appear to be independent of the level of theory employed. It should be noted, however, that the experimental C–O bonds in both Cyp_2-EN (1.4167(11) Å) and in Cy_2-EN (1.418(2) Å) (see Table 2) are shorter than the average C–O in secondary alcohols found in a survey of crystal structures in the Cambridge Structural Database (CSD) (1.432(11) Å) [74] and interestingly, this is precisely the sort of value predicted by the two DFT methods (see Table S1). On the other hand, the mean experimental C–C bond lengths of Cyp_2-EN and Cy_2-EN are as expected for bonds between sp^3 carbon atoms (the CSD average is 1.530(15) Å [74]) so the DFT calculations do indeed appear to slightly overestimate the C–C bond lengths in the ligands Cyp_2-EN and Cy_2-EN, although the calculated values are still within the standard deviation of the crystallographic data.

The addition of polarization functions had virtually no effect on the C–N and C–C bond lengths and caused a small increase in the C–O bond. The use of the CPCM/UAKS solvation model to simulate a condensed phase gave no obvious gain in accuracy at a significant expense of computational time.

Table 3
Comparison of selected bond angles between experimentally observed and theoretically computed structures in gas phase (GP) and solvent (CPCM) of three amino-alcohol ligands. Only differences (=calculated − experimental) are shown.

Bond angles (°)	C–N–C		O–C–C		N–C–C		C–C–C	
	GP	CPCM	GP	CPCM	GP	CPCM	GP	CPCM
BHEEN								
Experimental	112.74(8)		109.67(10)		109.7(3)			
X3LYP								
6-31G(d,p)	0.8		−2.3		0.2			
6-31+G(d,p)	0.9	−0.1	−2.1	−1.0	−0.2	0.4		
6-311++G(d,p)	1.0	0.0	−2.0	−1.0	−0.2	0.4		
PBEPBE								
6-31G(d,p)	0.4		−2.5		0.3			
6-31+G(d,p)	0.6	−0.5	−2.3	−1.1	−0.1	0.4		
6-311++G(d,p)	0.6	−0.4	−2.1	−1.1	−0.1	0.5		
Cy_2-EN								
Experimental	112.90(7)		113.1(1.0)		112.1(2.6)		104.2(1.6)	
X3LYP								
6-31G(d,p)	1.4		−0.8		0.1		0.2	
6-31+G(d,p)	1.5	0.7	−0.8	−0.9	0.3	0.4	0.2	0.3
6-311++G(d,p)	1.6	0.7	−0.8	−0.8	0.3	0.5	0.2	0.3
PBEPBE								
6-31G(d,p)	0.9		−0.7		0.1		0.1	
6-31+G(d,p)	1.1	0.2	−0.8	−0.8	0.2	0.4	0.2	0.2
6-311++G(d,p)	0.5	1.1	−0.8	−0.8	0.5	0.3	0.2	0.2
Cyp_2-EN								
Experimental	113.54(13)		109.96(57)		110.4(1.9)		111.15(66)	
X3LYP								
6-31G(d,p)	1.3		−0.8		−0.2		0.1	
6-31+G(d,p)	1.5	0.8	−0.8	−0.6	0.0	0.2	0.1	0.4
6-311++G(d,p)	1.5	0.7	−0.8	−0.6	0.0	0.2	0.1	0.4
PBEPBE								
6-31G(d,p)	0.8		−0.8		−0.2		0.1	
6-31+G(d,p)	1.0	−0.5	−0.8	−0.6	0.0	0.1	0.1	0.0
6-311++G(d,p)	1.0	0.2	−0.7	−0.6	0.0	0.2	0.0	0.0

Please cite this article in press as: P.R. Varadwaj et al., J. Mol. Struct. (THEOCHEM) (2009), doi:10.1016/j.theochem.2009.08.009

Table 4
Comparison of selected normal modes of vibration of three amino-alcohol ligands calculated at the X3LYP/6-311++G(d,p) and PBEPBE/6-311++G(d,p) levels of theory in the gas phase (GP) and with the CPCM solvation model, and the experimental resonance Raman and infrared spectra of the compounds in the solid state.[a]

	X3LYP (6-311++G(d,p))						PBEPBE (6-311++G(d,p))						Experimental								
	GP			CPCM			GP			CPCM			Raman				Infrared				Av expt
	Freq	Int	Calc/expt	Freq	Int	Calc/expt	Freq	Int	Calc/expt	Freq	Int	Calc/expt	Observed	Fitted			Observed	Fitted			
	cm^{-1}	km mol^{-1}		cm^{-1}	km mol^{-1}		cm^{-1}	km mol^{-1}		cm^{-1}	km mol^{-1}		Freq cm^{-1}	Appear	Freq cm^{-1}	Int %	Freq cm^{-1}	Appear	Freq cm^{-1}	Int %	cm^{-1}
BHEEN																					
OH str	3863	83	1.24	3594	434	1.15	3747	61.9	1.2	3468	380.3	1.11	3120	vw, br	3102	3	3105	m, br	3089	21	3113
NH str	3517	12.2	1.08	3362	88.8	1.03	3421	10.5	1.05	3256	84	1	3271	m	3270	17	3267	s	3267	47	3269
CH_2 asym str	3042	98.2	1.04	3004	104	1.02	2973	67	1.01	2921	101.5	1	2934	sh	2933	34	2934	sh			2934
	3038	103.8	1.04	2965	132.6	1.02	2965	110.1	1.02	2882	100.9	0.99	2912	s	2912	44	2930	w	2919	20	2921
CH_2 sym str	2953	164	1.03	2872	179.2	1.01	2874	175.4	1.01	2783	188	0.97	2856	vs	2857	100	2857	m	2855	20	2857
	2927	133.9	1.03	2851	144.1	1	2847	153.7	1	2760	166	0.97	2810	m	2806	32	2866	sh	2790	23	2838
NH bend + CH_2 scis	1516	97.9	1.02	1492	23.6	1	1454	106	0.97	1433	30.4	0.96	1497	m	1497	28	1489	w	1490	20	1493
NH bend + CH_2 scis	1507	12.5	1.02	1483	92.8	1.01	1448	8.5	0.98	1426	86.8	0.97	1470	sh	1468	8	1474	m	1475	19	1472
CH_2 twist + COH bend	1305	44.1	1.02	1297	53	1.02	1256	46.3	0.98	1246	49.8	0.98	1273	m	1273	30	1279	w	1278	18	1276
CN str	1162	79.8	1.03	1138	131.5	1.01	1135	38.6	1.01	1112	117.1	0.99	1125	w	1121	15	1126	m	1124	56	1126
CO str + CH_2 twist	1079	60.5	1.03	1065	98.9	1.01	1044	60.7	0.99	1032	85.6	0.98	1041	w	1042	14	1063	s	1062	100	1052
CC str + CN str	1053	114.1	1.11	1046	211.5	1.1	1026	114	1.08	1021	231	1.07	949	vw, br	940	3	955	vs	953	100	952
CH_2 rock	874	22.8	1.01	866	37.9	1	844	24.5	0.97	837	41.3	0.97	866	m	866	24	866	s	867	56	866
CH_2 rock	826	30.6	0.97	822	84	0.97	798	35.7	0.94	792	91.9	0.93					851	vs	850	90	851
NH deform + CH_2 twist	799	132.7	1.06	792	266	1.05	778	118.5	1.03	769	252.8	1.02					755	sh	740	22	755
OCCN torsion	539	16.9	0.97	534	31	0.96	523	15.7	0.94	518	30.4	0.94	554	vw	550	3					554
OH torsion	251	243	1.27	243	436	1.23	244	225.2	1.24	237	417.7	1.2	197	w	190	3					197
chain skeletal motion	195	5.1	1.63	187	34	1.56	189	4.4	1.58	182	30.3	1.52	120	m	116	17					120
Average calc/expt (>1000 cm^{-1})			*1.03(6)*			*1.01(4)*			*1.00(6)*			*0.98(4)*									
Average calc/expt (<1000 cm^{-1})			*1.15(24)*			*1.12(21)*			*1.11(23)*			*1.09(21)*									
Cyp_2-EN																					
OH str	3851	75.7	1.18	3592	458.7	1.10	3735	56.2	1.15	3464	423.8	1.06	3065	w, b	3065	1	3092	m b	3083	15	3079
NH str	3498	6.9	1.14	3335	83.6	1.08	3401	6.5	1.10	3213	85.3	1.04	3256	w	3255	11	3256	s	3255	39	3256
CH_2 asym str	3101	124.8	1.05	3088	165.4	1.04	3041	107	1.03	3027	138.7	1.02	2960	s	2957	100	2959	s	2959	27	2960
	3086	25.2	1.05	3070	25.3	1.05	3027	18.7	1.03	3009	34	1.03	2918	s	2934	19	2949	sh	2945	21	2934
	3071	31.1	1.05	3059	47	1.05	3013	30.5	1.03	3000	30	1.03	2903	sh	2916	62	2922	m	2910	19	2913
CH_2 sym str	3057	91	1.07	3047	112	1.06	2994	90.9	1.04	2981	110.9	1.04	2868	s	2867	62	2872	m	2869	18	2870
	3039	21.5	1.07	3017	100.6	1.06	2976	44.6	1.05	2941	87.7	1.03	2845	sh	2739	10					2845
CH_2 asym str (NCCN chain)	3044	87	1.07	2977	44.7	1.04	2972	24.7	1.04	2898	37.3	1.02	2856	sh	2849	42	2851	m	2847	13	2854
CH_2 sym str (NCCN chain)	2951	133.4	1.05	2875	172.8	1.02	2873	144.2	1.02	2784	188.1	0.99	2829	sh	2817	15	2789	sh	2784	12	2809
CH str	2993	66.4	1.06	2915	45.1	1.03	2914	70.5	1.03	2832	43.4	1.00			2831	23	2827	m	2822	12	2827
CH_2 scis	1527	3.7	1.03	1505	21.1	1.02	1469	3.6	0.99	1446	32.5	0.98	1472	sh	1473	16	1485	m	1485	28	1479
NH bend	1513	70.7	1.05	1499	84.9	1.04	1455	65.2	1.01	1444	59.6	1.00	1445	m	1445	30			1458	10	1445
CC str + CH + OH deform	1440	12.5	1.05	1424	17.4	1.03	1384	10.3	1.01	1369	16.9	0.99	1377	w	1377	12	1377	m	1376	41	1377
CH_2 wag	1320	20.8	1.05	1313	26.1	1.05	1266	17.2	1.01	1254	28.3	1.00	1255	vw	1257	6					1255
CC str + CH_2 twist	1247	29.9	1.05	1238	39	1.04	1202	25.3	1.01	1199	28.6	1.01	1194	w	1192	11	1179	vw, sh	1178	4	1187
CH_2 twist	1234	63.9	1.06	1223	93	1.05	1188	58.3	1.02	1176	76.5	1.01	1170	sh	1144	13	1150	m	1150	41	1160
CN str + CH_2 twist	1172	26.8	1.05	1162	13.3	1.04	1140	32.4	1.02	1127	93.4	1.01					1117	s	1117	83	1117
CO str + CC str + CN str	1072	167.3	1.11	1061	345.5	1.10	1061	11	1.10	1026	338.9	1.07			1004	12	962	s	962	96	962
CC str + CN str + CH_2 wag	1017	2.1	1.08	1013	21.6	1.07	992	18.9	1.05	983	27.4	1.04	953	w	953	10	937	m	937	56	945
CC str + CH_2 twist	948	17.8	1.05	944	30.1	1.04	920	15	1.02	909	29.6	1.00	907	m	907	44	905	m	904	40	906
CC str + CH_2 twist + NH deform	862	43.4	1.05	858	111.3	1.05	841	46.5	1.02	837	139.4	1.02	821	w	820	12	820	m	819	43	821

Please cite this article in press as: P.R. Varadwaj et al., J. Mol. Struct. (THEOCHEM) (2009), doi:10.1016/j.theochem.2009.08.009

NH deform + CH_2 rock	802	78.9	1.02	792	192.3	1.01	780	69.3	1.00	772	136	0.99					783	sh	787	13	783
CH_2 rock (chain)	772	3.4	1.03	769	11.2	1.03	746	4.8	1.00	745	35.7	1.00	746	vw	746	3					746
NCCN ring deform	561	21.3	1.04	561	41.9	1.04	541	19.7	1.00	549	40.8	1.02	540	m	541	21					540
OH deform	241	67.9	1.45	228	353	1.37	233	3363	1.40	225	320.4	1.36	166	w	166	15					166
NCCN chain + ring deform	165	6.8	1.38	159	21.6	1.33	160	6.2	1.33	157	17.4	1.31	120	s	120	86					120
Average calc/expt (>1000 cm^{-1})			*1.07*(*5*)			*1.05*(*3*)			*1.04*(*5*)			*1.02*(*3*)									
Average calc/expt (<1000 cm^{-1})			*1.13*(*16*)			*1.12*(*12*)			*1.10*(*16*)			*1.09*(*14*)									
Cy_2-EN																					
OH str	3847	61.4	1.26	3579	439.7	1.17	3728	40.9	1.22	3448	397.9	1.13	3040	w br	3060	1	3086	m br	3078	13	3063
NH str	3515	23	1.08	3404	94.9	1.04	3412	23.9	1.05	3296	91.9	1.01	3265	w	3267	8	3265	s	3265	24	3265
CH_2 asym str	3074	95.4	1.04	3056	151.5	1.03	3010	89.9	1.02	2995	178.5	1.01	2949	s	2950	75	2970	w	2968	3	2960
	3062	142.6	1.04	3053	145.7	1.04	3002	100.2	1.02	2990	135.7	1.02			2940	50	2941	sh	2940	19	2941
	3057	116.9	1.05	3049	155.8	1.04	2998	102.8	1.03	2988	75.9	1.02	2924	s	2923	56	2924	s	2923	40	2924
	3049	88	1.05	3036	120.1	1.05	2990	85.9	1.03	2974	109.8	1.03	2881	m	2889	32	2907	w	2893	9	2894
CH_2 asym str (NCCN chain + ring)	3046	39.3	1.07	3007	123	1.05	2974	49.9	1.04	2943	114.9	1.03	2850	s	2851	100	2855	m br	2852	27	2853
CH_2 sym str (ring)	3022	47.3	1.07	3002	43.3	1.07	2957	48.6	1.05	2938	52.3	1.04	2814	sh	2819	15	2821	w	2817	6	2818
CH str (of CHO group)	2983	55.3	1.07	2903	49.1	1.04	2903	66	1.04	2809	53.2	1.01	2770	sh	2773	5	2795	w	2767	41	2783
CH str (of ring connecting N)	2898	99.3	1.07	2711	61	1.00	2815	117.2	1.04	2593	67.3	0.96	2658	w	2660	5	2762	sh	2735	3	2710
NH deform + CH_2 scis	1525	99.3	1.06	1498	99.7	1.04	1465	100	1.02	1437	85.3	1.00	1445	m	1444	13	1435	w	1435	10	1440
CH_2 scis (ring)	1507	8	1.08	1496	14.2	1.07	1448	9	1.04	1436	25.7	1.03	1394	vw	1396	2	1398	vw br	1399	10	1396
CH_2 wag + CH deform (connecting CHO)	1397	15.6	1.03	1386	15.1	1.02	1338	16.5	0.99	1326	15.8	0.98	1348	w	1347	11	1358	m br	1357	21	1353
CH_2 wag + CH deform	1371	17.2	1.05	1367	28.3	1.05	1317	10.6	1.01	1312	23.5	1.00	1302	w	1302	12	1310	w	1312	22	1306
CH_2 twist + CH_2 wag + CH deform	1353	4	1.08	1345	13.4	1.08	1300	6.2	1.04	1289	19.7	1.03	1244	w	1245	14	1252	w	1252	18	1248
CH_2 twist + CH deform + OH def	1286	10.5	1.06	1279	16.1	1.05	1242	11.8	1.02	1234	20.5	1.02	1207	w	1209	12	1219	m	1219	35	1213
CH deform + OH deform + CH_2 twist	1256	21.7	1.05	1245	266	1.04	1212	14.9	1.02	1201	17.5	1.01	1190	w	1190	9	1196	m	1196	26	1193
CH_2 twist (chain) + CH deform + NH def	1242	55.6	1.08	1232	63.7	1.08	1195	56	1.04	1185	60.7	1.03	1142	w	1143	10	1148	m	1147	35	1145
OH deform + CC str + CH_2 twist	1191	55.7	1.06	1185	85	1.05	1149	48.3	1.02	1143	74.2	1.02	1122	vw	1124	5	1128	m	1128	40	1125
CN str + CH_2 rock + CH_2 twist + CH_2 wag	1158	42.1	1.04	1042	182.6	0.94	1119	2.9	1.01	1112	117.3	1.00	1107	vw	1107	9	1115	m	1115	32	1111
CC str + OH deform	1093	13.5	1.01	1089	8.1	1.00	1070	2.03	0.99	1066	4.2	0.98	1088	vw	1088	7	1082	s	1081	95	1085
CO str + CC str	1085	49.1	1.01	1075	75.4	1.00	1051	30.5	0.98	1042	42.3	0.97	1074	vw	1076	5					1074
CO str + CC str	1064	23.3	1.01	1056	29.1	1.00	1034	23.5	0.98	1026	16.3	0.97	1059	m	1059	14	1057	m	1056	50	1058
CC str + OH deform + CH_2 twist + CH_2 wag	1055	25	1.02	1053	54.8	1.01	1026	14.6	0.99	1023	46.6	0.99	1043	vw	1045	3	1032	sh	1026	16	1038
OH str + CC str + CN str	1036	102	1.01	1025	222	1.00	1007	135.9	0.98	997	275.7	0.97	1028	m	1028	14	1020	m	1021	44	1024
CC str + CH_2 wag	963	2.2	1.00	961	4.6	1.00	943	2.3	0.98	941	4.1	0.98	957	w	957	9	964	s	964	77	961
CH_2 rock	935	8.5	1.00	931	23	1.00	902	8.6	0.97	897	22.3	0.96	926	vw	926	4	939	s	939	60	933
CH_2 twist	901	0.9	0.98	803	2	0.88	880	1.7	0.96	881	1.8	0.96	916	vw	914	3	916	s	916	94	916
NH deform + CC str + CH_2 wag + CH_2 rock	871	40.8	0.98	869	87.5	0.98	844	35.4	0.95	842	75	0.95	891	vw	891	2	891	w	891	15	891
CC str + CH_2 rock	857	25.5	1.02	855	49.2	1.01	829	25.6	0.98	827	50.5	0.98	845	m	845	23	841	s	842	100	843
CC str + CH_2 rock	843	34.4	1.03	840	85.7	1.02	821	46.5	1.00	817	117.6	0.99					822	s	821	54	822
NH deform + CH_2 rock (chain)	812	46.2	1.03	801	82.8	1.02	789	32.3	1.00	778	74.2	0.99	781	m	782	16	795	m	792	31	788
CH_2 rock + NH deform	573	10.2	0.95	573	14.8	0.95	552	12.1	0.91	552	19.5	0.91	604	w	605	6					604
ring deform + CH_2 rock	555	36	1.01	555	75.5	1.01	537	33.1	0.97	538	72.3	0.97	552	m	553	21					552
(ring + chain) deform	490	2.5	1.02	487	5.7	1.01	476	2.1	0.99	473	5	0.98	482	vw	485	4					482
ring deform (torsion)	447	9.4	1.01	447	16.8	1.01	434	8.8	0.98	434	16.6	0.98	443	m	444	12					443
ring deform (torsion)	434	2.1	1.04	434	4	1.04	420	1.7	1.01	421	3.2	1.01	417	m	417	9					417
Ring deform	336	1	0.93	390	3.3	1.08	420	1.7	1.16	377	3.2	1.04	361	w	360	5					361
HO deform + NCCN chain deform	279	52.4	1.37	275	192.6	1.35	272	44.1	1.34	267	189.8	1.32	203	w	203	2					203
OH deform	252	154	1.48	257	232.5	1.51	238	141	1.40	247	210	1.45	170	w	171	7					170
(ring + chain) deform	185	1.3	1.23	187	0.5	1.24	179	1.1	1.19	181	0.3	1.20	151	m	151	10					151
NCCN deform	166	8.9	1.38	160	23	1.33	161	8.3	1.34	155	22.6	1.29	120	m	120	11					120
Average calc/expt (>1000 cm^{-1})			*1.06*(*5*)			*1.04*(*4*)			*1.03*(*5*)			*1.01*(*3*)									
Average calc/expt (<1000 cm^{-1})			*1.09*(*17*)			*1.08*(*17*)			*1.07*(*16*)			*1.06*(*16*)									

[a] *Abbreviations used:* str = stretching, asym = asymmetric, sym = symmetric, bend = bending, rock = rocking, scis = scissoring, twist = twisting, wag = wagging, deform = deformation.

Please cite this article in press as: P.R. Varadwaj et al., J. Mol. Struct. (THEOCHEM) (2009), doi:10.1016/j.theochem.2009.08.009

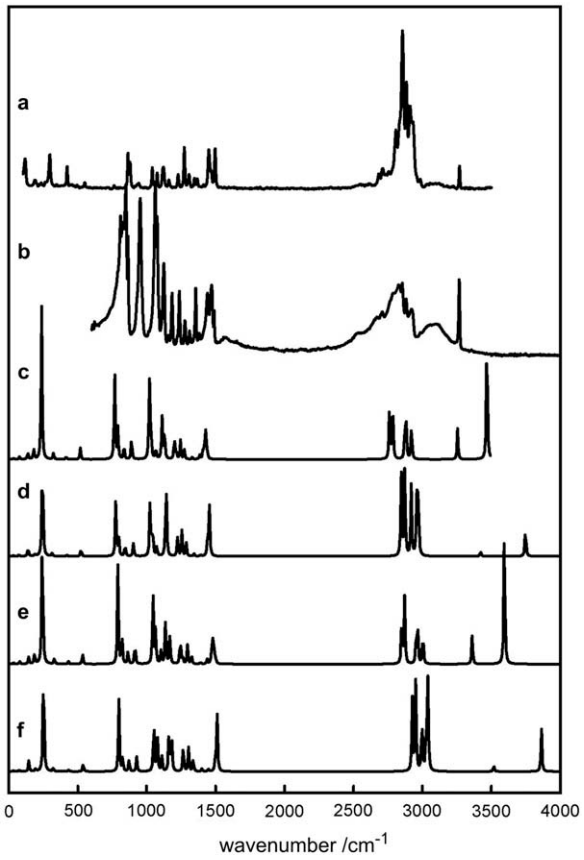

Fig. 2. The vibrational spectra of BHEEN. The experimental spectra are (a) Raman and (b) IR. The calculated spectra are from (c) PBEPBE/6-311++G(d,p) with the CPCM/UAKS solvation model, (d) PBEPBE/6-311++G(d,p) in the gas phase, (e) X3LYP/6-311++G(d,p) (CPCM/UAKS) and (f) X3LYP/6-311++G(d,p) (gas phase).

The PBEPBE functional gave a longer C–O bond length than X3LYP and virtually identical results for the C–N and C–C bond lengths. In general, an excellent agreement between the computed and the experimental valence bond angles (Table 3) was also obtained for all combinations studied. Except for the bond angle O–C–C in BHEEN (and that may be an artifact of comparing the geometry of the neutral and the protonated ligand) all the other angles agree to about one degree. Errors in bond length of up to 0.02 Å and errors in bond angle of around 1° are typical for DFT calculations for molecules with first- and second-row elements [75]. Hence, if the main aim is the prediction of molecular structures, then the use of the larger basis sets and solvation models appears to be unnecessary and calculations at the X3LYP/6-31G(d,p) level of theory appear to be adequate for these compounds.

3.2. Vibrational spectra

In Table 4 we compare the most important normal mode harmonic vibrational frequencies obtained from DFT calculations with those of the experimentally measured bands of the three ligands; a full comparison is given in Table S2 of the Supplementary Information. Both the infrared and the Raman spectra were deconvoluted by fitting with the smallest possible number of Lorentzian functions using standard non-linear least squares methods. The fitted frequencies and their intensity, relative to the most intense band in the spectrum, are also listed in Table 4. The experimental spectra were assigned by comparison with the spectra of ethanolamine [76] and of cyclohexanol [77], with the help of a standard reference [78] and by matching the computationally calculated band intensities with the experimentally-observed ones. The calculated normal modes were visualized using GaussView 03 [23]. Fig. 2 shows the experimental spectra and the calculated spectra of BHEEN; Figure S1 of the Supplementary Information shows a portion of its resonance Raman spectrum fitted with a number of Lorentzian functions. In virtually all cases there is a close agreement between the apparent position of each band in the spectrum and the position of the Lorentzian function used to fit the band. For convenience, therefore, we have used the experimental values in our analysis.

Table 5
Average values of the electron density (ρ_{BCP}) and the Laplacian of charge density ($\nabla^2 \rho_{BCP}$) at the important open shell and close-shell bond critical points and ring critical points in the three amino-alcohols.

	X3LYP/6-31G(d,p)		PBEPBE/6-31G(d,p)	
	ρ_{BCP} (au)*	$\nabla^2 \rho_{BCP}$ (au)	ρ_{BCP} (au)	$\nabla^2 \rho_{BCP}$ (au)
O–H	0.367(1)	−2.049(6)	0.359(1)	−1.944(7)
O–C	0.253(2)	−0.478(11)	0.251(2)	−0.514(8)
N–C	0.273(1)	−0.779(11)	0.268(1)	−0.712(1)
N–H	0.342(1)	−1.76(12)	0.333(1)	−1.673(11)
H–C	0.278(1)	−0.953(11)	0.269(1)	−0.881(8)
C–C	0.251(6)	−0.593(36)	0.244(6)	−0.543(33)
	ρ_{RCP} (au)*	$\nabla^2\rho_{RCP}$ (au)	ρ_{RCP} (au)	$\nabla^2\rho_{RCP}$ (au)
Cyclopentyl	0.0368	0.2468	0.0373	0.2443
Cyclohexyl	0.0174	0.1118	0.0179	0.1117

*1 au of ρ = 6.7483 eÅ^{-3}, and 1 au of $\nabla^2 \rho$ = 24.099 eÅ^{-5}.

Given the complexity of the spectra and the fact that many bands overlap (especially above 2500 cm^{-1}) there is some uncertainty in the assignments and many of these (Table S2) are tentative. Nevertheless, it is clear that the DFT methods employed generally reproduce the spectra well. A notable difference between the predicted and the observed spectra is the O–H stretching frequency. In free alcohols the O–H stretching frequency is observed as a sharp line between about 3590 and 3650 cm^{-1} [78]. The DFT calculations predict this to occur at about 3850 cm^{-1} or 3740 cm^{-1} in the gas phase (X3LYP and PBEPBE, respectively) and 3590 cm^{-1} and 3460 cm^{-1} in a simulated solvent environment. The observed band is broad and centered around 3080 cm^{-1}, characteristic of the involvement of the OH group in hydrogen bonding. This is indeed seen in the crystal structures of these compounds (as will be discussed elsewhere [13]) where, for instance, a short (<2 Å) inter-molecular contacts between the hydroxyl group and N-atom of different molecules is observed in lattices of Cyp_2-EN and Cy_2-EN. It is reasonable to assume that the network of H-bonds in crystal lattices of the three ligands influenced the position of bands in the vibrational spectra not only in the case of the OH groups, but also of other fragments, particularly around N-atoms. Because of this, the direct comparison of computed and experimental bands in Table 4 must be treated with caution.

Anderson and Udval, using largely the training set of Pople et al. [79], examined the basis set dependence of frequency calculations using B3LYP [80]; for basis sets of between 6-311G(d,p) and 6-311++G(3df,3pd) quality scaling factors of 0.9679 and 1.0100 were recommended for normal and low-frequency vibrations, respectively. These correspond to calculated:observed frequency ratios of 1.033 and 0.9901, respectively. In a comprehensive examination of the performance of computational methods in calculating fundamental, low-frequency and zero point vibrational energies, Radom et al. [81] showed that DFT methods perform well and recommend the use of Becke's three- and one-parameter hybrid functionals such as B3LYP and B1LYP and the modifications to Becke's B-97 hybrid functional such as B972. For B3LYP, scaling factors for the calculation of fundamental vibrational frequencies were found to have converged at a basis set of 6-311G(d) quality, although convergence is slower for low-frequency vibrations. In

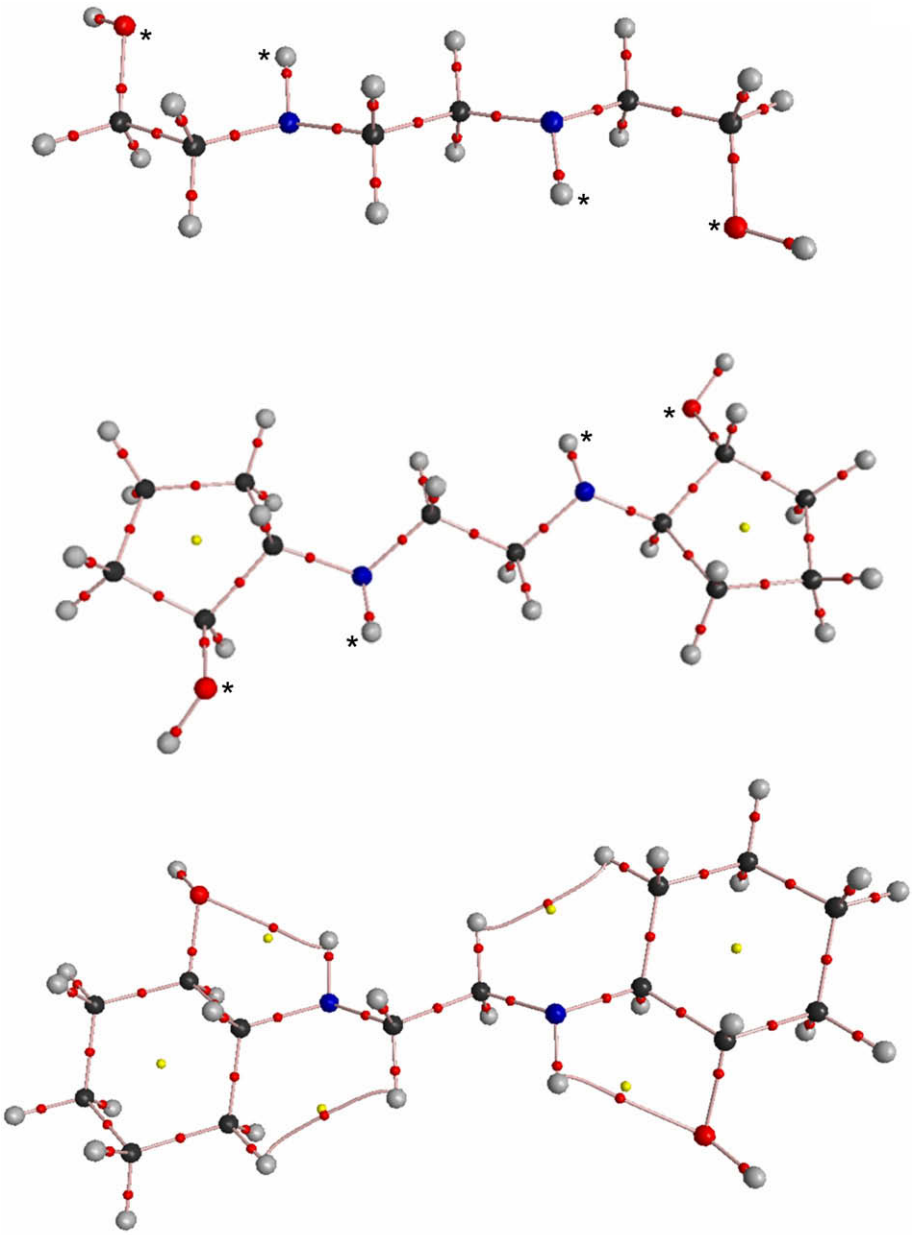

Fig. 3. Representation of the AIM analysis of BHEEN, Cyp_2-EN and Cy_2-EN showing bond critical points (small spheres along the bond paths) and ring critical points (small spheres inside the bond rings). The structures were determined with X3LYP/6-31G(d,p).

Table 6
NBO computed second-order stabilization energy $E^{(2)}$ caused by the charge transfer between indicated orbitals and selected structural parameters of the three ligands obtained from X3LYP and PBEPBE functionals combined with either 6-31G(d,p) or 6-31+G(d,p) basis set.

Compound	Charge transfer between orbitals[a]	Second-order energy $E^{(2)}$ (kcal mol^{-1})				O···HN bond distance (Å)				O···H–N angle (°)			
		X3LYP		PBEPBE		X3LYP		PBEPBE		X3LYP		PBEPBE	
		6-31G(d,p)	6-31+G(d,p)	6-31G(d,p)	6-31+G(d,p)	6-31G(d,p)	6-31+G(d,p)	6-31G(d,p)	6-31+G(d,p)	6-31G(d,P)	6-31+G(d,p)	6-31G(d,P)	6-31+G(d,p)
BHEEN	LP(2) O23 → BD*(1) N1–H15 and LP(2) O25 → BD*(1) N2–H16	0.84	0.72	0.96	0.78	2.398	2.448	2.383	2.441	105.0	105.9	103.4	103.9
Cyp_2-EN	LP(2) O38 → BD*(1) N37–H40 and LP(2) O18 → BD*(1) N17–H20	0.60	0.59	0.62	0.60	2.531	2.562	2.515	2.552	104.9	105.6	104.0	104.4
Cy_2-EN	LP(2) O44 → BD*(1) N43–H46 and LP(2) O21 → BD*(1) N20–H23	1.74	1.55	1.84	1.62	2.244	2.263	2.230	2.253	110.8	111.5	110.1	110.5

[a] LP and BD* denotes lone-pair of electrons and anti-bonding orbital, respectively.

Please cite this article in press as: P.R. Varadwaj et al., J. Mol. Struct. (THEOCHEM) (2009), doi:10.1016/j.theochem.2009.08.009

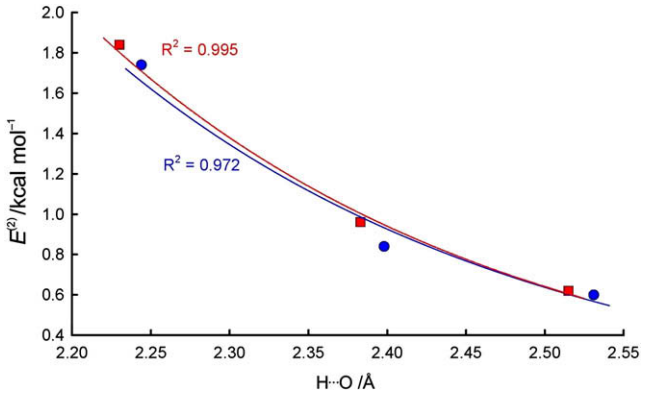

Fig. 4. Dependence of the second-order perturbation lowering energy ($E^{(2)}$) from charge transfer between the alcoholic O-atom and the N–H anti-bonding orbitals in amino-alcohols based on structures generated by X3LYP (circles) and PBEPBE (squares) using a 6-31G(d,p) basis set on the intra-molecular H-bond distance. The data were fitted with an exponential function.

the case of B3LYP/6-311+G(d,p), scaling factors of 0.9688 (calculated:observed = 1.032) and 1.0189 (calculated:observed = 0.9815) are recommended for fundamental and low-frequency calculations, respectively. Ratios of calculated:observed frequencies of 1.01–1.06 are typical for DFT methods [82–85]. We observe that, in general, incorporation of the CPCM/UAKS technique improved the prediction of the vibrational frequencies (but no gain in accuracy was observed for structural parameters, bond lengths and angles, as discussed above) and that the PBEPBE functional performed significantly better than X3LYP in this regard. Thus, the average ratio of calculated:observed frequencies (for frequencies >1000 cm^{-1}) for PBEPBE/6-311++G(d,p)/CPCM are 0.98(4), 1.02(3) and 1.01(3) for BHEEN, Cyp_2-EN and Cy_2-EN, respectively.

The generally good agreement between the computed and experimental structural and vibrational data suggests that the computed structures are reliable and gives credence to conclusions arrived at from an analysis of the topology of the electron density (see below). This will be particularly important in analyzing metal–ligand complexes as obtaining diffraction quality crystals of these ligands with a variety of metal ions has proved to be a formidable task. We believe that computed vibrational frequencies, particularly those involving groups that include or are near the N- and O-donor atoms, will provide us with additional insight and understanding of the chemistry between the metal ions and the amino-alcohol ligands.

3.3. QTAIM analysis

The Quantum Theory of Atoms in Molecules of Bader [21] has been utilized to explore various possible interactions in a molecular system and its ability to identify these interactions between inter-atomic regions in terms of bond critical points (BCPs) and the formation of ring surfaces characterized by ring critical points (RCPs) is well documented [86–89]. We used QTAIM analysis to determine whether weak interactions occur in the DFT structures of these three amino-alcohols since these interactions may influence the affinity and selectivity of these ligands towards metal ions. Since we have shown that the 6-31G(d,p) basis set is sufficient to accurately reproduce the solid state structures of these ligands, we focused our QTAIM analysis on structures obtained mainly with this basis set. The values of the electron density, $\rho(r)$, and its Laplacian, $\nabla^2\rho(r)$, at the bond and ring critical points are listed in Table S3 of the Supplementary Information and, for illustration purposes, representative values of BCPs and RCPs are summarized in Table 5.

The electron density at the BCP usually correlates with the strength of the bond between two atoms. Values of $\rho_{BCP} < 0.10$ au are indicative of a closed-shell (i.e., predominantly non-covalent) interaction [90]; it is usually accompanied by a relatively small and positive value of $\nabla^2\rho_{BCP}$ [91]. By contrast, for a shared (i.e., predominantly covalent) interaction, ρ_{BCP} is usually >0.1 au [90] (or >0.15 au [92]) and $\nabla^2\rho_{BCP}$, which may be positive or negative [90] (but usually negative [92]), is typically of the same order as ρ_{BCP}. As seen in Table 5, the values for the covalent framework are consistent with the covalent character of these bonds ($\rho(r) > 0.2$ au and $\nabla^2\rho(r) < 0$). Examples of the molecular graphs for the structures obtained with the X3LYP functional are shown in Fig. 3.

It is seen from Fig. 3 that the QTAIM analysis of BHEEN and Cyp_2-EN did not predict any weak intra-molecular interactions. For example, (see Fig. 1) no H-bonding was identified between atoms marked with an asterisk, namely (N1)H15 and O23 or (N2)H16 and O25 in BHEEN, and between (N17)H20 and O18, and (N37)H40 and O38 in Cyp_2-EN) even though one of the necessary conditions for the existence of such weak interactions, namely the N–H···O distance criterion, is satisfied. To illustrate this point, the distance between the H-atom on nitrogen and alcoholic oxygen in BHEEN and Cyp_2-EN at the X3LYP/6-31G(d,p) level of theory is 2.398, 2.531 Å and 2.518, 2.731 Å in the computed and crystallographic structures, respectively. The computed distances are significantly shorter than the sum of the van der Waals radii of H (1.20 Å) and O (1.52 Å); the experimental values are larger and this can be attributed to the strong inter-molecular H-bonds in which the H-atom on the OH group is involved in. It has been demonstrated recently that an inter-atomic distance smaller than the sum of the van der Waals radii is a necessary but not sufficient condition for bond formation because the directional exchange interaction may dominate over non-directional classical electrostatic interactions [89]. In such a case the distance rule is invalid and examples of atoms that bond preferentially to others that are further, rather than to closer neighbors, are known [93]. In contrast, in Cy_2-EN there is indeed a typical intra-molecular H-bond resulting from the interaction between (see Fig. 1) (N43)H46 and alcoholic oxygen O44, N–H···O, with a bond path between these two atoms and a BCP (seen as a dot in Fig. 3) indicative of an additional localized stabilizing contribution to the overall energy of Cy_2-EN (and, as expected because of the centrosymmetric nature of the molecule the same is observed between (N20)H23 and O21). The values of (i) ρ_{BCP} of this H-bond (0.0168 and 0.0175 au from the X3LYP and PBEPBE wavefunctions, respectively) and (ii) $\nabla^2\rho$ (0.0679 and 0.0672 au, respectively) are small and positive, diagnostic of a predominantly electrostatic interaction. It is noteworthy that (i) both functionals predicted the formation of the intra-molecular H-bonds only in Cy_2-EN, and (ii) PBEPBE, which generated better quality Raman spectra, predicted the value of ρ_{BCP} of this H-bond to be somewhat larger than that obtained from X3LYP. The H-bonding in Cy_2-EN results in the formation of a 5-member ring with a RCP that is located close to the BCP of the hydrogen bond, indicative of the weakness of the N–H···O interaction. Using a larger basis set (6-311++G(d,p), for example) with both functionals causes this weak interaction to disappear.

There is an additional and more persistent intra-molecular interaction discovered only in Cy_2-EN (Fig. 3), namely a C–H···H–C interaction or H–H bond [86] between H37 and H42 (and between H14 and H19). It was predicted with both functionals with two smallest basis sets employed (interestingly, the H-bond was predicted only with the smallest basis set used, 6-31G(d,p)). The presence of the H–H bonds results in formation of two additional 6-member rings with the requisite RCPs. The average H···H distance obtained in the gas phase from the three basis sets is 2.226(5) and 2.228(4) Å when PBEPBE and X3LYP were used,

respectively. The equivalent distances in the structures generated in a simulated solvent environment from 6-31+G(d,p) and 6-311++G(d,p) are 2.206(1) and 2.207(7) Å when PBEPBE and X3LYP were used, respectively. There is therefore excellent agreement between the computed and experimental (2.204 Å) distances.

As mentioned above, classically this kind of intra-molecular interaction, when identified in metal complexes, has been interpreted as a destabilizing steric repulsion responsible for the decrease in stability of the complex. If these close contacts between H atoms were indeed contributing to *destabilization* of the molecule, their persistence in the free ligands in the gas phase is difficult to explain.

A bond path in a QTAIM analysis indicates the presence of a preferred quantum-mechanical exchange channel and the interatomic exchange-correlation energy always stabilizes the local interaction [89]. These short contacts would be classically viewed as H···H steric repulsive interactions. The values of ρ_{BCP} (0.0087 and 0.0088 au from the X3LYP/6-31G(d,p) and PBEPBE/6-31G(d,p) wavefunctions, respectively) and $\nabla^2\rho_{BCP}$ (0.0360 and 0.0359 au, respectively) for this H–H interaction are smaller than those found for the H-bond. This results in a RCP being very close to the BCP of the H–H bond (Fig. 3). The stabilization may not be negligible; it has been demonstrated that for ρ_{BCP} values in the range of 0.01 au (as is the case here) the formation of a H–H bond has a stabilizing effect of up to 10 kcal mol^{-1} [86]. This pairwise additive stabilization does not depend on the attractive or repulsive nature of the classical interaction between the atoms' charge densities. Whether the overall energy of the system decreases as a result of the H–H bond depends on the relative magnitude of the energies of the classical and quantum mechanical interaction.

Our QTAIM analysis does not predict the formation of equivalent H–H bonds in Cyp_2-EN even though the distance criterion is met. It suggests that the presence of a 5m-RR alters the intramolecular interactions in the molecule. It is seen in Table 5 that ρ_{RCP} and $\nabla^2\rho_{RCP}$ of the cyclopentyl moiety in Cyp_2-EN are twice as large as those of the cyclohexyl moiety in Cy_2-EN. One might speculate that the increased electron density *within* the 5-member ring is responsible for the absence of the preferential quantum-mechanical exchange channels between atoms that meet the distance criterion (as discussed above for Cyp_2-EN) and hence no intra-molecular H-bonds and H–H bonds are observed in this molecule. This may be important in explaining the differences in their solution chemistry where Cyp_2-EN has a significantly smaller affinity for metal ions than Cy_2-EN [20]. We shall address this issue elsewhere.

3.4. NBO analysis

We attempted to verify the existence of these weak interactions by performing an NBO analysis on the X3LYP/6-31G(d,p) and PBEPBE/6-31G(d,p) structures since QTAIM alone does not give the origin of these interactions. H-bond formation is presumed to stem from an $n(O) \rightarrow \sigma^*(NH)$ charge delocalization. However, there are other factors such as electrostatic, polarization, and dispersion interactions that result in the net stabilization of the H-bonding contacts, but NBO analysis does not provide a separate estimate of these components. The computed values of $E^{(2)}$, together with some structural parameters applicable either to the demonstrated H-bonds (in Cy_2-EN) or to the molecular fragments where H-bonds would be expected to form, as discussed above for BHEEN and Cyp_2-EN, are listed in Table 6. The NBO analysis predicts an electron exchange between appropriate orbitals and non-zero values of $E^{(2)}$ for all three ligands. One might therefore argue that H-bonding does occur in all three, and that the strength of the H-bond is in the order Cy_2-EN > BHEEN > Cyp_2-EN, an order that is consonant with a decrease in the N–H···O distance (Fig. 4) and is preserved by both functionals and all basis sets. The QTAIM analysis only indicated H-bonding in Cy_2-EN presumably because its analysis is focused on identifying bonds due to computed preferential quantum-mechanical exchange bond paths as discussed above.

Increasing the size of the basis set to 6-311++G(d,p) causes values of $E^{(2)}$ for BHEEN and Cyp_2-EN to decrease below 0.5 kcal mol^{-1} (the default cut-off significance level in the NBO analysis) whilst the hydrogen bond is still observed in Cy_2-EN with $E^{(2)}$ values of 0.71 and 0.80 kcal mol^{-1} at the X3LYP/6-311++G(d,p) and PBEPBE/6-311++G(d,p) level, respectively. Thus, whilst the magnitude of $E^{(2)}$ is basis set dependent and marginally dependent on whether a hybrid or a pure GGA functional is used, the trend Cy_2-EN > BHEEN > Cyp_2-EN is preserved, suggesting that this is indeed a true physical property of these ligands.

It is interesting to note that the same trend is observed when the strength of metal complexes with these three ligands is analysed [20] (Table 1), log K_{ML}(Cy_2-EN) > log K_{ML}(BHEEN) > log K_{ML}(Cyp_2-EN) for any given M(II) ion. Since the donor atoms are the same in the three ligands, and the only change in their structure is the presence of 5m-RR in Cyp_2-EN and a 6m-RR in Cy_2-EN compared with BHEEN, it is clear that the presence of these rings influences complex stability. Since the formation of a complex implies an exchange of electron density between the donor atoms of the ligand and the metal ion, and since the second-order stabilization energy $E^{(2)}$ discussed above is directly related to the donor atoms in the three ligands, it might be tentatively concluded that the ability of the ligand to transfer charge between orbitals as indicated in Table 6, and that is described by $E^{(2)}$, is a factor that influences its ability to form complexes with metal ions. We are currently studying the structure of these ligands with metal ions and hope to establish whether this is an important factor in determining the stability of their metal ion complexes.

The NBO analysis did not identify the weak H–H bond in Cy_2-EN (Fig. 3) predicted by the QTAIM analysis. As we pointed out above, the RCP and BCP are close to each other and hence this interaction is presumably below the 0.5 kcal mol^{-1} significance threshold in Gaussian 03.

We briefly investigated the effect of a solvent (water) on these weak interactions by performing an NBO analysis on the structures of the amino-alcohols determined with PBEPBE/6-31G(d,p) by incorporating the CPCM/UAKS technique. As was the case in the gas phase, we found no weak interactions for BHEEN and for Cyp_2-EN. However, the N–H···O hydrogen bond (but not the very weak H–H bond) in Cy_2-EN found in the gas phase persisted in water with $E^{(2)}$ = 0.7 kcal mol^{-1}.

4. Summary

The geometries of the three amino-alcohol ligands were energy-minimized both at the RX3LYP and RPBEPBE levels of theory in conjunction with three basis sets, 6-31G(d,p), 6-31+G(d,p), and 6-311++G(d,p) under C_i point group symmetry. Both the methods predicted bond lengths within the standard deviation of available crystallographic data. They overestimated C–O and C–C bond lengths (by up to 0.02 Å), but the C–N bond lengths were reproduced to better than 0.01 Å. The calculated C–C and C–N bond lengths appear to be independent of the level of theory employed. The addition of polarization functions had a negligible effect on the bond lengths and the use of the CPCM/UAKS solvation model gave no obvious gain in accuracy. An excellent agreement between the computed and the experimental bond angles was also obtained for all combinations studied. As with bond lengths, the use of a larger basis set or the simulation of a condensed phase, offered no significant improvement in valence angles.

However, incorporation of the CPCM/UAKS technique improved the prediction of the vibrational frequencies; the PBEPBE functional performed significantly better than X3LYP in this regard with the average ratios of calculated to observed frequencies (>1000 cm^{-1}) of 0.98(4), 1.02(3) and 1.01(3) for BHEEN, Cyp_2-EN and Cy_2-EN, respectively.

To gain insight into the nature of the bonding interactions between atoms constituting the ligands, we have applied both QTAIM and NBO techniques to the wavefunctions of the energy-minimized structures. The QTAIM analysis of BHEEN and Cyp_2-EN did not predict intra-molecular interactions even though the geometric criterion (distance between two atoms being smaller than the sum of the atoms' van der Waals radii) was satisfied. Both functionals, but only with the 6-31G(d,p) basis set, predicted the formation of intra-molecular H-bonds in Cy_2-EN; PBEPBE, which generated better quality Raman spectra, predicted the value of ρ_{BCP} of this H-bond to be larger than that obtained from X3LYP. An additional and more persistent intra-molecular interaction in Cy_2-EN, namely a C–H···H–C interaction (or H–H bond) was also observed. It has been predicted with both functionals and the two smaller basis sets employed. The average H···H distance obtained in the gas phase in conjunction with the three basis sets is 2.226(5) and 2.228(4) Å when PBEPBE and X3LYP were used, respectively. The equivalent distances in the structures generated in a simulated solvent environment CPCM/UAKS obtained from 6-31+G(d,p) and 6-311++G(d,p) basis sets are 2.206(1) and 2.207(7) Å when PBEPBE and X3LYP were used, respectively; this is in excellent agreement with the experimental distance of 2.204 Å. Classically, this kind of intra-molecular interaction, when identified in metal complexes, is interpreted as a destabilizing steric repulsion responsible for the decrease in stability of the complex. We have rationalized the presence of the H- and a H–H bonds in Cy_2-EN and their absence in Cyp_2-EN in terms of differences in the values of ρ_{RCP} and $\nabla^2\rho_{RCP}$ of the 5-member and 6-member alkyl rings in Cyp_2-EN and Cy_2-EN, respectively. As expected, the open shell and closed shell interactions in these ligands are characterized by $\rho_{BCP} > 0$, $\nabla^2\rho_{BCP} < 0$ and $\rho_{BCP} > 0$, $\nabla^2\rho_{BCP} > 0$, respectively. These interactions disappeared when we enlarged the size of the basis set to 6-311++G(d,p), indicative of the importance of an appropriate selection of a basis set for the study of weak interactions.

The NBO analysis of the second-order perturbation lowering energy ($E^{(2)}$) (from charge transfer between the alcoholic O-atom and the N–H anti-bonding orbitals in all three amino-alcohols) suggests that there are indeed weak N–H···O interactions in all the ligands. These are clearly evident when 6-31G(d,p) and 6-31+G(d,p) basis sets were used but their magnitude decreases when the size of the basis set was increased to 6-311++G(d,p). The strength of the intra-molecular H-bond between the amino and alcohol functionalities in these amino-alcohols follows the trend Cy_2-EN > BHEEN > Cyp_2-EN that mimics the trend, log K_{ML}(Cy_2-EN) > log K_{ML}(BHEEN) > log K_{ML}(Cyp_2-EN), observed when the strength of metal complexes involving Cu^{2+} (r = 0.57 Å), Ni^{2+} (r = 0.69 Å), and Cd^{2+} (r = 0.95 Å) with these three ligands is analyzed. We suspect that the ability of these ligands to form intra-molecular interactions may influence the strength of their complexes with metal ions; we are currently investigating this and will report our findings elsewhere.

Acknowledgements

P.R.V. thanks I.C. for an appointment as a post-doctoral fellow, rewarding support and funding during this work. I.C. gratefully acknowledges financial support from the National Research Foundation and the University of Pretoria. H.M.M. thanks the South African Research Chairs Initiative of the Department of Science and Technology administered by the National Research Foundation, the Mellon Foundation through grants administered by the University of the Witwatersrand, and the University Research Committee of the University of the Witwatersrand for funding.

Appendix A. Supplementary data

Supplementary data associated with this article can be found, in the online version, at doi:10.1016/j.theochem.2009.08.009.

References

[1] D.R. Schaad, in: D. Ager (Ed.), Handbook of Chiral Chemicals, second ed., CRC Press, Boca Raton, FL, 2005, p. 443.
[2] D.T. Wong, F.P. Bymaster, E.A. Engleman, Life Sci. 57 (1995) 411.
[3] S.J. Kwon, S.Y. Ko, Tetrahedron Lett. 43 (2002) 639.
[4] D.J. Ager, I. Prakash, D.R. Schaad, Chem. Rev. 96 (1996) 835.
[5] J.R. Dehli, V. Gotor, Tetrahedron: Asymm. 11 (2000) 3693.
[6] G. Cardillo, C. Tomasini, Chem. Soc. Rev. 25 (1996) 117.
[7] R. Noyori, M. Kitamura, Angew. Chem. Int. Ed. Engl. 30 (1991) 49.
[8] M. Kitamura, S. Suga, H. Oka, R. Noyori, J. Am. Chem. Soc. 120 (1998) 9800.
[9] S. Wang, S.J. Trepanier, J.C. Zheng, Z. Pang, M.J. Wagner, Inorg. Chem. 31 (1992) 2118.
[10] S. Wang, K.D.L. Smith, Z. Pang, M.J. Wagner, J. Chem. Soc., Chem. Commun. (1992) 1594.
[11] A.S. de Sousa, R.D. Hancock, J. Chem. Soc., Chem. Commun. (1995) 415.
[12] A.S. de Sousa, R.D. Hancock, J.H. Reibenspies, J. Chem. Soc. Dalton Trans. (1997) 2831.
[13] A.S. de Sousa, M.A. Fernandes, K. Padayachy, S.A. Reisinger, D. Sannasy, H. M. Marques, unpublished results.
[14] A.E. Martell, R.D. Hancock, Metal Complexes in Aqueous Solution, Plenum Press, New York, 1996.
[15] R.D. Hancock, Pure Appl. Chem. 58 (1986) 1445.
[16] R.D. Hancock, Analyst 122 (1997) 51R.
[17] A.S. de Sousa, G.J.B. Croft, C.A. Wagner, J.P. Michael, R.D. Hancock, Inorg. Chem. 30 (1991) 3525.
[18] A.S. de Sousa, R.D. Hancock, J.H. Reibenspies, J. Chem. Soc., Dalton Trans. (1997) 939.
[19] R.D. Hancock, A.S. de Sousa, G.B. Walton, J.H. Reibenspies, Inorg. Chem. 46 (2007) 4749.
[20] V. Uwamariya, MSc Dissertation, University of the Witwatersrand, 2005.
[21] R.F. Bader, Atoms in Molecules: A Quantum Theory, Oxford University Press, Oxford, 1990.
[22] M.J. Frisch, G.W. Trucks, H.B. Schlegel, G.E. Scuseria, M.A. Robb, J.R. Cheeseman, J.J.A. Montgomery, T. Vreven, K.N. Kudin, J.C. Burant, J.M. Millam, S.S. Iyengar, J. Tomasi, V. Barone, B. Mennucci, M. Cossi, G. Scalmani, N. Rega, G.A. Petersson, H. Nakatsuji, M. Hada, M. Ehara, K. Toyota, R. Fukuda, J. Hasegawa, M. Ishida, T. Nakajima, Y. Honda, O. Kitao, H. Nakai, M. Klene, X. Li, J.E. Knox, H.P. Hratchian, J.B. Cross, C. Adamo, J. Jaramillo, R. Gomperts, R.E. Stratmann, O. Yazyev, A.J. Austin, R. Cammi, C. Pomelli, J.W. Ochterski, P.Y. Ayala, K. Morokuma, G.A. Voth, P. Salvador, J.J. Dannenberg, V.G. Zakrzewski, S. Dapprich, A.D. Daniels, M.C. Strain, O. Farkas, D.K. Malick, A.D. Rabuck, K. Raghavachari, J.B. Foresman, J.V. Ortiz, Q. Cui, A.G. Baboul, S. Clifford, J. Cioslowski, B.B. Stefanov, G. Liu, A. Liashenko, P. Piskorz, I. Komaromi, R.L. Martin, D.J. Fox, T. Keith, M.A. Al-Laham, C.Y. Peng, A. Nanayakkara, M. Challacombe, P.M.W. Gill, B. Johnson, W. Chen, M.W. Wong, C. Gonzalez, J.A. Pople, Gaussian 03, Revision D.01, Gaussian Inc., Wallingford CT, 2004.
[23] R. Dennington, T. Keith, J. Millam, K. Eppinnett, W.L. Hovell, R. Gilliland, GaussView, 3.09, Semichem, Inc., Shawnee Mission, KS, 2003.
[24] X. Xu, W.A. Goddard, Proc. Natl. Acad. Sci. USA 101 (2004) 2673.
[25] X. Xu, W.A. Goddard, J. Phys. Chem. A 108 (2004) 2305.
[26] X. Xu, Q. Zhang, R.P. Muller, W.A. Goddard, J. Chem. Phys. 122 (2005) 014105.
[27] C. Lee, W. Yang, R.G. Parr, Phys. Rev. B 37 (1988) 785.
[28] J.P. Perdew, K. Burke, M. Ernzerhof, Phys. Rev. Lett. 77 (1996) 3865.
[29] J.P. Perdew, K. Burke, M. Ernzerhof, Phys. Rev. Lett. 78 (1997) 1396.
[30] Y. Zhao, J. Pu, B.J. Lynch, D.G. Truhlar, Phys. Chem. Chem. Phys. 4 (2004) 673.
[31] V.N. Staroverov, G.E. Scuseria, J. Tao, J.P. Perdew, J. Chem. Phys. 119 (2003) 12129.
[32] A.D. Boese, M.L. Martin, N.C. Handy, J. Chem. Phys. 119 (2003) 3005.
[33] S. Moon, D.A. Case, J. Comput. Chem. 27 (2006) 825.
[34] M.D. Liptak, G.C. Shields, Int. J. Quantum Chem. 105 (2005) 580.
[35] P.J. Stephens, J.F. Devlin, C.F. Chabalowski, M.J. Frisch, J. Phys. Chem. 98 (1994) 11623.
[36] N. Díaz, D. Suárez, K.M. Merz, Chem. Phys. Lett. 326 (2000) 288.
[37] J.N. Harvey, Annu. Rep. Prog. Chem., Sect. C 102 (2006) 203.
[38] K. Müller-Dethlefs, P. Pavel Hobza, Chem. Rev. 100 (2000) 143.
[39] Z. Latajka, Y. Bouteiller, J. Chem. Phys. 101 (1994) 9793.
[40] G. Chung, O. Kwon, Y. Kwon, J. Phys. Chem. A 102 (1998) 2381.
[41] M. Masella, J.P. Flament, J. Chem. Phys. 110 (1999) 7245.
[42] C. Van Alsenoy, K. Siam, J.D. Ewbank, L. Schäfer, J. Mol. Struct. (THEOCHEM) 136 (1986) 77.
[43] C.F.P. Silva, M.L.T.S. Duarte, R. Fausto, J. Mol. Struct. 482 (1999) 591.

[44] I. Hyla-Kryspin, G. Haufe, S. Grimme, Chem. Eur. J. 10 (2004) 3411.
[45] B. Hammer, L.B. Hansen, J.K. Nørskov, Phys. Rev. B 59 (1999) 7413.
[46] Y. Zhang, W. Yang, Phys. Rev. Lett. 80 (1998) 890.
[47] S.N. Maximoff, J.E. Peralta, V. Barone, G.E. Scuseria, J. Chem. Theory Comput. 1 (2005) 541.
[48] L. Onsager, J. Am. Chem. Soc. 58 (1936) 1486.
[49] O. Tapia, O. Goscinski, Mol. Phys. 29 (1975) 1653.
[50] S. Miertus, E. Scrocco, J. Tomasi, Chem. Phys. 55 (1981) 117.
[51] S. Miertus, J. Tomasi, Chem. Phys. 65 (1982) 239.
[52] J. Tomasi, M. Persico, Chem. Rev. 94 (1994) 2027.
[53] C.J. Cramer, D.G. Truhlar, Chem. Rev. 99 (1999) 2161.
[54] D.M. Chipman, J. Phys. Chem. A 106 (2002) 7413.
[55] C.-G. Zhan, J. Bentley, D.M. Chipman, J. Chem. Phys. 108 (1998) 177.
[56] A. Klamt, G. Schüürmann, J. Chem. Soc., Perkin Trans. 2 (1993) 799.
[57] J. Andzelm, C. Kölmel, A. Klamt, J. Chem. Phys. 103 (1995) 9312.
[58] V. Barone, M. Cossi, J. Phys. Chem. A 102 (1998) 1995.
[59] M. Cossi, V. Barone, J. Chem. Phys. 109 (1998) 6246.
[60] M. Cossi, N. Rega, G. Scalmani, V. Barone, J. Comput. Chem. 24 (2003) 669.
[61] A.D. McLean, G.S. Chandler, J. Chem. Phys. 72 (1980) 5639.
[62] R. Krishnan, J.S. Binkley, R. Seeger, J.A. Pople, J. Chem. Phys. 72 (1980) 650.
[63] J. Wang, R. Wolf, J.W. Caldwell, P.A. Kollman, D.A. Case, J. Comput. Chem. 25 (2004) 1157.
[64] HYPERCHEM, 7.03, Hypercube, Inc., Gainesville, FL, 2002.
[65] J.J.P. Stewart, J. Comput. Chem. 10 (1989) 209.
[66] T.A. Keith, AIMAll, 08.05.04, http://aim.tkgristmill.com, 2008.
[67] F. Biegler-König, J. Schönbohm, D. Bayles, AIM2000, 1, http://www.gauss.fh-bielefeld.de/aim2000.
[68] F. Biegler-König, J. Schönbohm, D. Bayles, J. Comp. Chem. 22 (2002) 545.
[69] N.-B. Wong, Y.-S. Cheung, D.-Y. Wu, Y. Ren, A. Tian, W.-K. Li, J. Phys. Chem. A 104 (2000) 6077.
[70] O.E. Taurian, R.H. Contreras, J. Mol. Struct. (THEOCHEM) 504 (2000) 119.
[71] P.R. Varadwaj, I. Cukrowski, H.M. Marques, J. Phys. Chem. A 112 (2008) 10657.
[72] F. Weinhold, in: P.v.R. Schleyer, N.L. Allinger, T. Clark, J. Gasteiger, P.A. Kollman, H.F. Schaefer, P.R. Schreiner (Eds.), Encyclopedia of Computational Chemistry, vol. 3, John Wiley & Sons, Chichester, 1998, p. 1792.
[73] E.E. Glendening, A.E. Reed, J.E. Carpenter, F. Weinhold, NBO (Natural Bond Orbital), 3.0, as implemented in GAUSSIAN 03, Gaussian Inc., Pittsburg, 2004.
[74] F.H. Allen, O. Kennard, D.G. Watson, L. Brammer, A.G. Orpen, R. Taylor, J. Chem. Soc., Perkin Trans. II (1987) S1.
[75] C.W. Bauschlicher, A. Ricca, H. Partridge, S.R. Langhoff, in: D.P. Chong (Ed.), Recent Advances in Density Functional Methods Part II, World Scientific, Singapore, 1997, p. 165.
[76] N.A. Macleod, J.P. Simons, Phys. Chem. Chem. Phys. 6 (2004) 2821.
[77] D.W. James, H.F. Shurvell, R.M. Parry, J. Raman Spectros. (1976) 201.
[78] E. Pretsch, P. Buhlmann, C. Affolter, Structure Determination of Organic Compounds, Springer-Verlag, Berlin, 2000.
[79] B.G. Johnson, P.M.W. Gill, J.A. Pople, J. Chem. Phys. 98 (1993) 5612.
[80] M.P. Andersson, P. Uvdal, J. Phys. Chem. A 109 (2005) 2937.
[81] J.P. Merrick, D. Moran, L. Radom, J. Phys. Chem. A 111 (2007) 11683.
[82] G. Rauhut, P. Pulay, J. Am. Chem. Soc. 117 (1995) 4167.
[83] A.P. Scott, L. Radom, J. Phys. Chem. 100 (1996) 16502.
[84] J. Baker, A.A. Jarzecki, P. Pulay, J. Phys. Chem. A 102 (1998) 1412.
[85] Y. Tantirungrotechai, K. Phanasant, S. Roddecha, P. Surawatanawong, V. Sutthikhum, J. Limtrakul, J. Mol. Struct. (THEOCHEM) 760 (2006) 189.
[86] C.F. Matta, J. Hernandez-Trujillo, T.-H. Tang, R.F.W. Bader, Chem. Eur. J. 9 (2003) 1940.
[87] S.J. Grabowski, A. Pfitzner, M. Zabel, A.T. Dubois, M. Palusiak, J. Phys. Chem. B 108 (2004) 1831.
[88] C.F. Matta, N. Castillo, R.J. Boyd, J. Phys. Chem. A 109 (2005) 3669.
[89] M. Pendás, E. Francisco, M.A. Blanco, C. Gatti, Chem. Eur. J. 13 (2007) 9362.
[90] R.F.W. Bader, H. Essén, J. Chem. Phys. 80 (1984) 1943.
[91] R.G.A. Bone, R.F.W. Bader, J. Phys. Chem. 100 (1996) 10892.
[92] M.F. Bobrov, G.V. Popova, V.G. Tsirelson, Russ. J. Phys. Chem. 80 (2006) 584.
[93] V. Luaña, A.M. Pendás, A. Costales, G.A. Carriedo, F.J. García-Alonso, J. Phys. Chem. A 105 (2001) 5280.

Please cite this article in press as: P.R. Varadwaj et al., J. Mol. Struct. (THEOCHEM) (2009), doi:10.1016/j.theochem.2009.08.009